Variable temperature study of the crystal and magnetic structures of the giant magnetoresistant materials *L*MnAsO (*L* = La, Nd)

N. Emery, E. J. Wildman, J. M. S. Skakle, and A. C. Mclaughlin*
The Chemistry Department, University of Aberdeen, Meston Walk, Aberdeen, AB24 3UE, Scotland

R. I. Smith
ISIS facility, RAL, Chilton, Didcot, Oxon OX11 0QX, United Kingdom

A. N. Fitch
European Synchrotron Radiation Facility, F-39043 Grenoble, France
(Received 13 January 2011; revised manuscript received 8 February 2011; published 29 April 2011)

A variable temperature neutron and synchrotron diffraction study has been performed on the giant magnetoresistant oxypnictides *L*MnAsO (*L* = La, Nd). The low-temperature magnetic structures have been studied, and results show a spin reorientation of the Mn^{2+} spins below T_N (Nd) for NdMnAsO. The Mn^{2+} spins rotate from alignment along *c* to alignment into the basal plane, and the Mn^{2+} and Nd^{3+} moments refine to 3.54(4) μ_B and 1.93(4) μ_B, respectively, at 2 K. In contrast, there is no change in magnetic structure with temperature for LaMnAsO. There is no evidence of a structural transition down to 2 K; however, discontinuities in the cell volume and *L*-O and Mn-As bond lengths are detected at ∼150 K for both materials. This temperature coincides with the electronic transition previously reported and suggests a coupling between electronic and lattice degrees of freedom.

DOI: 10.1103/PhysRevB.83.144429 PACS number(s): 61.05.F−, 75.47.De, 75.50.Ee, 71.20.Nr

I. INTRODUCTION

High-temperature superconductivity (HTSC) in layered cuprates with transition temperatures (T_c) >35 K (Ref. 1) has been extensively studied in the past 30 years. Recently, HTSC has been reported in a noncuprate material, the 1111-type pnictides *L*FeAsO (Ref. 2) with a maximum T_c of 55 K being achieved via substitution of oxygen with fluorine[3–5] or by creating oxygen vacancies.[6] The Fe-based parent compound crystallizes with the tetragonal ZrCuSiAs structure (space group *P*4/*nmm*). Below ∼155 K a structural distortion occurs, changing the symmetry of the cell from tetragonal to orthorhombic. This is followed by a spin-density-wave-type (SDW) antiferromagnetic (AFM) ordering of Fe^{2+} moments at $T_N = 137$ K.[7] Substitution of F^- onto the O^{2-} site or the presence of oxygen vacancies increases the number of charge carriers in the two-dimensional FeAs planes, producing a superconducting state that suppresses both the AFM and structural transition. Superconductivity was found to be induced not only by electron doping, but also by hole doping via substitution on the rare-earth site with Sr^{2+}.[8,9]

Partial substitution of Fe in $LaFe_{1-x}M_xAsO$ (*M* = Ni, Co, and Mn) has also been performed, promoting superconductivity in the case of Ni and Co.[10,11] When the system contains 11% Co, AFM ordering is destroyed and superconductivity is induced with a T_c of 14.3 K. LaONiAs exhibits bulk superconductivity with $T_c \sim 2.75$ K.[12] In contrast, LaCoAsO is an itinerant ferromagnet with a magnetic moment of 0.52 μ_B ($T_{Curie} \sim 66$ K)[13] and displays the characteristics of a "good" metal, with low room-temperature resistivity. Recent studies performed on its analog, NdCoAsO, showed similar magnetic behavior, with a higher magnetic transition of 85 K.[14] Neutron-diffraction data revealed that the Co spins order ferromagnetically in the *ab* plane below this temperature, with a small moment of 0.3 μ_B. The ordering of Nd^{3+} spins arises below 9 K, doubling the magnetic cell along the *c* axis, with AFM coupling of adjacent ferromagnetic planes. A subsequent study on this compound revealed a third magnetic transition at ∼3 K related to further AFM ordering of larger Nd moments.[15]

Superconductivity has been reported in the similar 122 family of $A_{1-x}B_xM_2As_2$ (*A* = K, Cs; *B* = Ba, Sr, Ca; *M* = Fe, Ni).[16–20] Comparable electronic and magnetic properties are apparent between the 122 and 1111 family, with $BaCo_2As_2$ (Refs. 18 and 21) bearing ferromagnetic character and $SrFe_2As_2$ and $BaFe_2As_2$ exhibiting a SDW.[17,22] $BaMn_2As_2$ is unique to other compounds in this family, as it is nonmetallic with an elevated T_N of 625 K.[23,24] We recently reported the electronic and magnetic properties of *L*MnAsO (*L* = La, Nd),[25] which are antiferromagnetic with $T_N = 317$ and 335 K for *L* = La and Nd, respectively. Both compounds display semiconducting behavior in addition to giant magnetoresistance (GMR), suggesting strong spin-charge coupling of the $3d^5$ electrons. In this paper, we present a variable temperature neutron diffraction study of *L*MnAsO (*L* = La, Nd) and show that a spin reorientation of the Mn^{2+} moments arises below T_N (Nd^{3+}). A synchrotron x-ray diffraction study of *L*MnAsO (*L* = La, Nd) has also been performed, and the results demonstrate that the electronic transition previously reported[25] is coupled to the crystal lattice.

II. EXPERIMENTAL

Polycrystalline samples of *L*MnAsO (*L* = Nd, La) were synthesized via a two-step solid-state reaction. Pieces of rare earth (Aldrich 99.9%) and As (Alfa Aesar 99.999%) were initially reacted at 900 °C in a quartz tube sealed under vacuum. "As-prepared" samples were then synthesized by reacting stoichiometric amounts of MnO_2 and Mn powders

(Aldrich 99.99%) with the presynthesized *L*As. All powders were ground under an inert atmosphere and pressed into pellets of 10-mm diam. A sintering step at 1150 °C for 48 h was employed, also in an evacuated quartz tube. Such as-prepared samples were found to be nominally Nd nonstoichiometric. Two more Nd stoichiometric samples were prepared by the reaction of an excess of 2% and 3% Nd powder, with stoichiometric amounts of NdAs, MnO_2, and Mn.

Powder x-ray diffraction patterns of *L*MnAsO (L = Nd, La) were collected using a Bruker D8 Advance diffractometer with twin Gobel mirrors and Cu $K\alpha$ radiation. Data were collected over the range $10 < 2\theta < 100$, with a step size of 0.02°, and could be indexed on a tetragonal unit cell of space group $P4/nmm$, characteristic of the *LM*AsO family (M = Fe, Ni, Co).[5]

Time-of-flight (TOF) neutron-diffraction patterns were recorded on the high-intensity diffractometer POLARIS at the pulsed neutron source ISIS facility, Rutherford Appleton Laboratory, UK. Samples were inserted into an 8-mm vanadium can, and data were collected between 2 and 400 K. Rietveld refinement[26] using the GSAS package[27] was carried out in order to determine the nuclear and magnetic structures of both compounds above and below T_N (Mn). Data were excluded between 2.1- and 2.3-Å d spacing, due to peaks from the sample environment.

Powder synchrotron x-ray diffraction patterns of *L*MnAsO (L = Nd and La) were recorded on ESRF beamline ID31 between 5 and 290 K. A wavelength of 0.39996 Å was used, and the sample was contained in a 0.5-mm-diam borosilicate glass capillary mounted on the axis of the diffractometer, about which it was spun at ~1 Hz to improve the powder averaging of the crystallites. Diffraction patterns were collected over the angular range 2°–45° 2θ and rebinned to a constant step size of 0.002° for each scan. The high-angle parts of the pattern were scanned several times to improve the statistical quality of the data in these regions. A small amount of MnAs impurity [1.5(1) wt %] was observed and fitted for NdMnAsO. A small amount of Nd_2O_3 [1.3(1) wt %] was also detected.

III. RESULTS AND DISCUSSION

A. Magnetic structure

It has recently been shown that *L*MnAsO (L = La, Nd) is a local moment antiferromagnet.[25] A weak ferromagnetic component was evidenced from superconducting quantum interference device (SQUID) magnetometry measurements; however, it is possible that this is due to MnAs impurities, as observed previously in magnetometry measurements of antiferromagnetic $BaMn_2As_2$.[24] The 290-K magnetic structure has been resolved from neutron-diffraction data[25] for *L*MnAsO (L = La, Nd). At 290 K (101) and (100), magnetic reflections are observed that can be indexed with a propagation vector $\mathbf{k} = (0,0,0)$, leading to identical magnetic and nuclear cells. Hence, the Mn^{2+} moments are aligned antiferromagnetically in the ab plane, but ferromagnetically along c, and the moment is ordered parallel to the c axis (Fig. 1). At 290 K, the Mn^{2+} moment refines to 2.43(1) μ_B and 2.35(2) μ_B for LaMnAsO and NdMnAsO, respectively. These magnetic reflections were not observable at 400 K, which is above

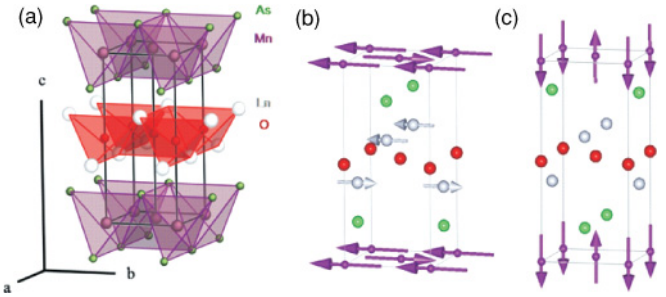

FIG. 1. (Color online) (a) Crystal structure, (b) 2-K magnetic structure of NdMnAsO, and (c) 290-K magnetic structure of *L*MnAsO (L = La, Nd).

the magnetic ordering temperature determined from SQUID magnetometry measurements. Upon cooling to 2 K, there is no change in crystal structure, and a good Rietveld fit is obtained to the tetragonal space group $P4/nmm$ at all temperatures (Fig. S1 in the supplementary material[28]). Tables SI and SII in the supplementary material show agreement factors, cell parameters, selected bond lengths, and angles[28] (χ^2 values are <1 below 290 K as a result of the small sample volume and sample environment from the cryostat). There is no change in the magnetic structure for LaMnAsO as the temperature is reduced to 2 K, and the moment is observed to increase slowly from 2.43(2) μ_B at 290 K to 3.34(2) μ_B at 2 K (Table SI in the supplementary material). The saturated moment is comparable to that reported for $BaMn_2As_2$ (Ref. 23) and is reduced from the theoretical value of 5 μ_B/Mn^{2+} as a result of a substantial hybridization between the Mn 3d and the As 4p orbitals.

A clear change in the intensities of the magnetic reflections is evidenced at 2 K for NdMnAsO (Fig. 2), which is below the temperature at which the Nd^{3+} spins are fully ordered antiferromagnetically [T_N (Nd) = 10 K], as observed previously from SQUID magnetometry measurements;[25] the (101) reflection is reduced compared to the (100), and an increase in intensity of the (102) peak is observed. All

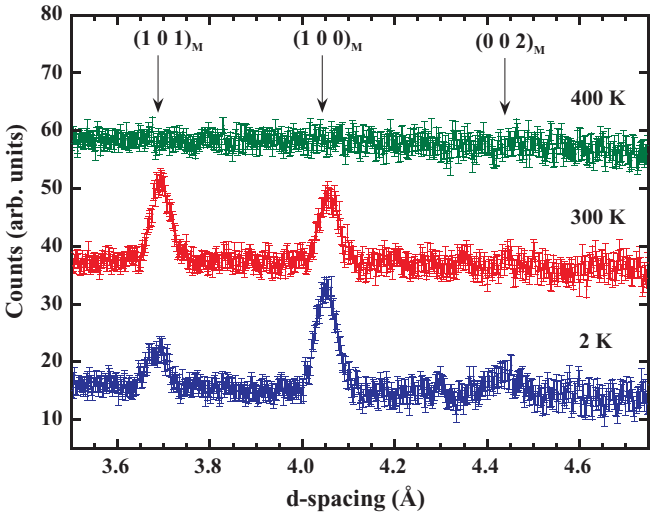

FIG. 2. (Color online) A portion of the POLARIS neutron diffraction pattern for NdMnAsO showing a change in magnetic diffraction as a result of antiferromagnetic Mn^{2+} ordering below 400 K and Nd^{3+} ordering below 10 K.

TABLE I. Basis vectors $[m_x,m_y,m_z]$ for the space group $P4/nmm$ with $\mathbf{k}=(0,0,0)$. Mn_1: ($^3/_4,^1/_4,^1/_2$), Mn_2: ($^1/_4,^3/_4,^1/_2$), Nd_1: ($^1/_4,^1/_4$,0.13034), and Nd_2: ($^1/_4,^1/_4$,0.86966).

Atom	Γ_2^1	Γ_3^1	Γ_6^1	Γ_9^2	Γ_{10}^2
Mn_1		$(0,0,m_z)$	$(0,0,m_z)$	$(m_x,m_y,0)$	$(m_x,m_y,0)$
Mn_2		$(0,0,m_z)$	$(0,0,-m_z)$	$(m_x,m_y,0)$	$(-m_x,-m_y,0)$
Nd_1	$(0,0,m_z)$	$(0,0,m_z)$		$(m_x,m_y,0)$	$(m_x,m_y,0)$
Nd_2	$(0,0,-m_z)$	$(0,0,m_z)$		$(m_x,m_y,0)$	$(-m_x,-m_y,0)$

reflections could be indexed with the primitive unit cell, so that $\mathbf{k}=(0,0,0)$. In order to determine the symmetry-allowed magnetic structures, symmetry analysis was undertaken using version 2 K of the software SARA*h*-representational analysis.[29] These calculations allow the determination of the symmetry-allowed magnetic structure that can result from a second-order transition, given the crystal structure prior to the transition and the propagation vector of the magnetic ordering. Only symmetry elements g that leave the propagation vector $\vec{k}$ invariant are considered: These form the little group G_k. The magnetic representation of a crystallographic site can be decomposed in irreducible representations Γ (IRs) of G_k.

First, we consider the case where just the Mn^{2+} spins are ordered, as observed for LaMnAsO below 317 K and NdMnAsO at 290 K. The different IRs obtained are displayed in Table I, and the allowed solutions correspond to two ferromagnetic and two antiferromagnetic models. The two ferromagnetic IRs can be easily ruled out as there is no evidence of a ferromagnetic contribution to the nuclear Bragg reflections. The best fit to the neutron data is obtained with the magnetic moment along c (i.e., IR Γ_6^1), as shown in Fig. S1 in the supplementary material.[28]

The magnetic structure of NdMnAsO changes at low temperature as a result of Nd^{3+} spin ordering (Fig. 2). The IRs associated to the Nd site are also presented in Table I. The decompositions are $\Gamma_{mag}=1\Gamma_3^1+1\Gamma_6^1+1\Gamma_9^2+1\Gamma_{10}^2$ and $\Gamma_{mag}=1\Gamma_2^1+1\Gamma_3^1+1\Gamma_9^2+1\Gamma_{10}^2$ for the Mn and Nd sites, respectively. In the case of a second-order phase transition, Landau theory states that only a single IR becomes critical, which leaves three IRs common to both sites: $1\Gamma_3^1$, $1\Gamma_9^2$, and $1\Gamma_{10}^2$, of which $1\Gamma_3^1$ and $1\Gamma_9^2$ are ferromagnetic, and $1\Gamma_{10}^2$ results in antiferromagnetic ordering of both Nd^{3+} and Mn^{2+}, as shown in Fig. 1(c). An excellent fit is obtained to this magnetic structure at 2 K (Fig. S1 and Table SII in the supplementary material[28]), and the refined magnetic moments of Mn^{2+} and Nd^{3+} are 3.54(4) μ_B and 1.93(4) μ_B, respectively. These results demonstrate that a spin reorientation arises below the Nd^{3+} antiferromagnetic transition so that the Mn^{2+} spins rotate from ordering parallel to c above T_N (Nd) to ordering in the basal plane below the Nd^{3+} spin transition, which demonstrates a strong coupling between the two sublattices. Such a spin reorientation transition has not been observed previously in any of the itinerant LMAsO (M = Fe, Co, Ni) systems,[7–13] and the most likely mechanism for the spin reorientation is competing single-ion anisotropy, as reported previously for L_2CuO_4.[30] The Mn^{2+} ion has $S=5/2$ and orbital angular momentum $L=0$, so that the preferred moment orientation is along c. The Nd^{3+} moment with $S=3/2$ and $L=6$ aligns preferentially in the basal plane. When the Nd^{3+} spins order below 24 K, the single ion anisotropy dominates that of Mn^{2+}, so that the manganese spins reorient into the basal plane. The same spin reorientation is not observed for LaMnAsO, in which lanthanum does not order magnetically.

B. Crystal structure

Previous results have shown that both LaMnAsO and NdMnAsO exhibit a sizable negative magnetoresistance (–MR).[25] –MR is observed below 380 K and 360 K for NdMnAsO and LaMnAsO, respectively, and decreases slowly upon cooling, reaching a maximum of –24% and –11%, respectively, at 200 K. At 150 K (T_e) the –MR for NdMnAsO increases rapidly to zero; at the same time a subtle electronic transition is observed as a result of a crossover between two three-dimensional variable-range-hopping (VRH) states. The electronic transition is thought to arise due to a change in hopping, with hopping via multiple sites occurring at high temperature and hopping via two sites occurring below 150 K. If tunneling of the electrons occurs via more than two sites, then quantum destructive interference (QDI) is possible. Upon application of a magnetic field, the QDI is diminished, resulting in the −MR observed between 150 and 380 K for NdMnAsO.[25] Magnetoresistance arising from quantum interference is only observed in highly disordered semiconductors and changes slowly with temperature below the magnetic transition temperature,[31] as observed for LMnAsO. This is in contrast to the colossal magnetoresistance observed in $Mn^{3+/4+}$ perovskites, which exhibit a peak in −MR at $\sim T_c$.[32]

In order to see if the electronic transition at $T_e=150$ K is coupled to the crystal lattice, a variable temperature synchrotron study has been performed on LMnAsO (L = La, Nd) between 5 and 290 K. The synchrotron x-ray powder diffraction patterns of LMnAsO (L = La, Nd) were fitted by the Rietveld method[26] using the GSAS program.[27] The backgrounds were fitted using linear interpolation and the peak shapes were modeled using a pseudo-Voigt function. Our data confirmed that LMnAsO (L = La, Nd) crystallize in the ZrCuSiAs-type structure[5,33] [spin group $P4/nmm$ $a=4.11398(1)$ and 4.043959(7); $c=9.03044(2)$ and 8.87868(3) for L = La and

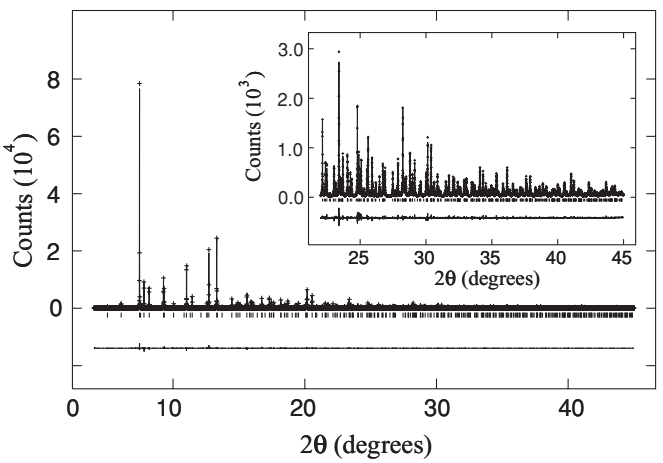

FIG. 3. Rietveld refinement fit to the 5-K ID31 synchrotron x-ray powder diffraction pattern of LaMnAsO.

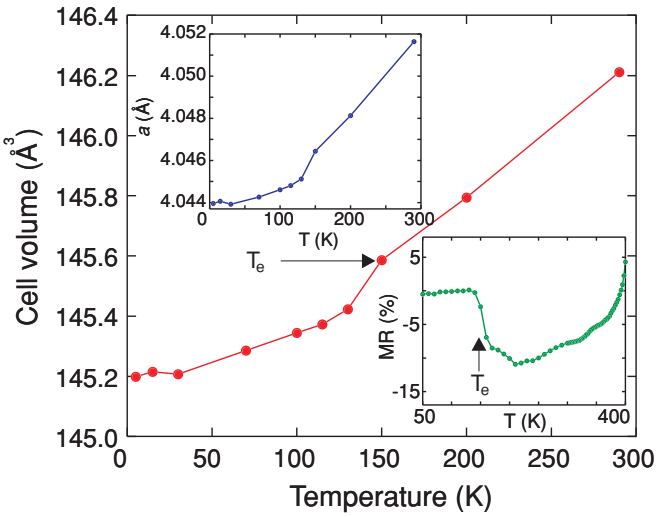

FIG. 4. (Color online) Variation of cell volume with temperature for NdMnAsO showing an anomaly at the electronic transition T_e. The insets show the temperature variation of the a cell parameter and the 5-T magnetoresistance.

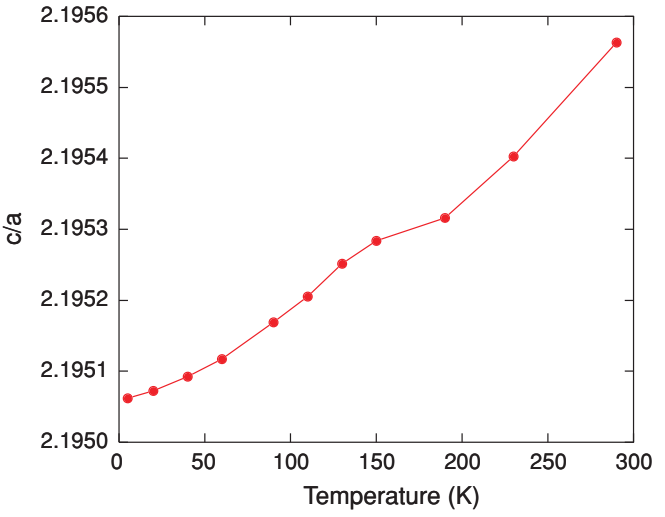

FIG. 5. (Color online) Temperature dependence of the c/a ratio for LaMnAsO.

Nd, respectively]. Unlike LMAsO (M = Fe, Co),[14] no orthorhombic distortion is observed down to 5 K. Excellent fits were obtained at all temperatures for both compounds as shown in Fig. 3 (Fig. S2 in the supplementary material[28]). The refinement results show that both compounds are anion stoichiometric and there is no evidence of cation or anion disorder. Nonstoichiometry on the L site is observed for both samples, so that the La and Nd occupancies refine to 0.966(2) and 0.970(2), respectively. Values of the agreement factors, refined cell parameters, and selected bond lengths and angles are displayed in Tables SIII and SIV in the supplementary material[28] for La and Nd, respectively.

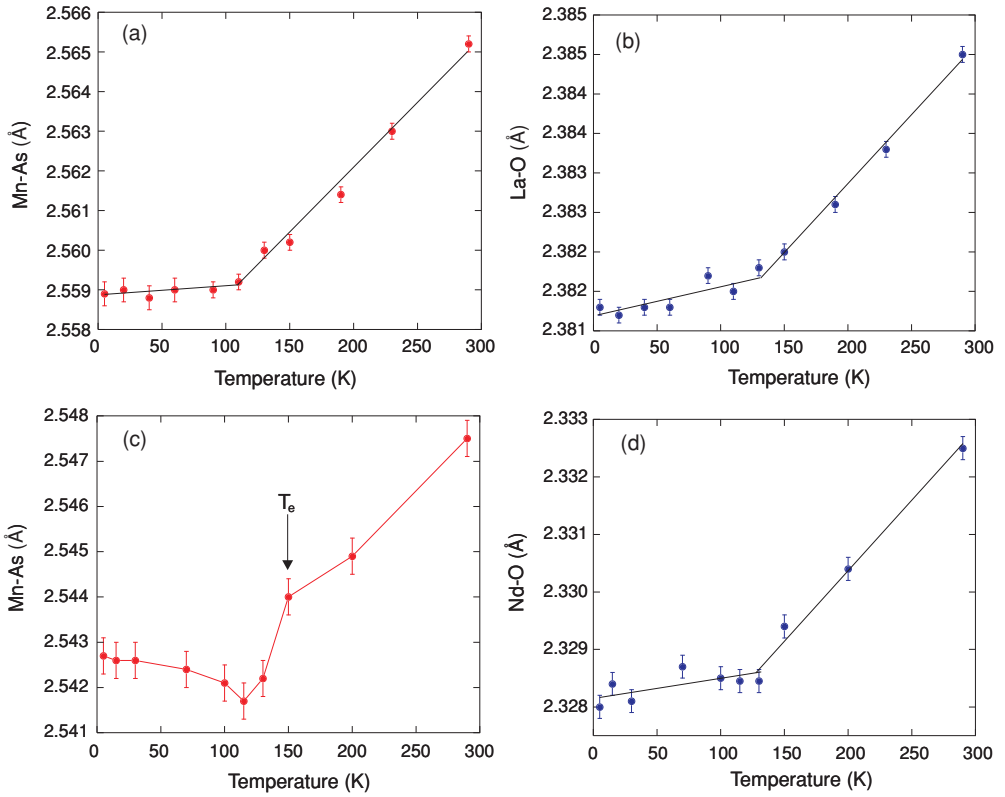

FIG. 6. (Color online) Temperature variation of (a) Mn-As bond length in LaMnAsO, (b) La-O bond distance, (c) Mn-As bond length in NdMnAsO, and (d) Nd-As bond distance.

Figure 4 shows the variation of cell volume and a with temperature for NdMnAsO, which show a clear discontinuity at T_e. The same anomaly is observed for LaMnAsO, although it is more subtle; Fig. 5 shows the variation of the c/a ratio for LaMnAsO, which demonstrates the same manifestation of T_e in the crystal lattice. Figure 6 shows the variation of the Mn-As and L-O bond lengths with temperature, and it is clear that the discontinuity in the cell volume is due to changes in these bond lengths at $\sim T_e$. The tetrahedral bond angles are displayed in Tables SIII and SIV in the supplementary material for LaMnAsO and NdMnAsO, respectively.[28] The results show that a reduction in La-O-La α_1 is observed with decreasing temperature while α_2 increases, so that at 5 K the angles are 119.49(1)° and 104.706(5)° for α_1 and α_2, respectively. In contrast both the Nd-O-Nd tetrahedral bond lengths are almost constant with temperature [$\alpha_1 = 120.58(1)°$ and $\alpha_2 = 104.219(4)°$ at 5 K]. The greater distortion in the Nd-O-Nd tetrahedral can be attributed to the larger bond mismatch between Mn-As and Nd-O in this material [Mn-As = 2.5427(3) Å and Nd-O = 2.3280(1) Å for NdMnAsO at 5 K, compared to Mn-As = 2.5589(3) Å and La-O = 2.3813(1) Å]. For both compounds, the α_2 As-Mn-As bond angles are almost temperature invariant, whereas the electronic transition T_e is manifest in the α_1 As-Mn-As tetrahedral bond angle. Electronic transitions such as the one reported for LMnAsO (Ref. 25) are well known in disordered semiconductors; for example, a crossover between two three-dimensional VRH states has previously been reported for $SrFeO_{3-\delta}$ (Ref. 34) and $Bi_{2.1}Sr_{1.93}Ca_{0.97-x}L_xCu_2O_{8+y}$ (L = Pr, Gd, Er).[35] The synchrotron x-ray refinement results demonstrate that the structural parameters are sensitive to subtle changes in the electronic state in LMnAsO, so that the electronic transition at 150 K is coupled to the crystal lattice. It has previously been shown that the electronic structure of LFeAsO systems strongly depends on small changes in interatomic distances and bond angles of the $FeAs_4$ units. The structural parameters control the electronic conduction band (due to the high degree of hybridization between Fe and As and also the Fe near- and next-nearest-neighbor interactions).[36] It would appear that the same may be true for the 1111 Mn^{2+} analog, and further studies of the electronic structure are warranted.

C. Stoichiometry studies

While writing this paper, we became aware of a recent paper by Marcinkova *et al*. that supports the low-temperature magnetic structure of NdMnAsO (Ref. 37) reported here. However, the electronic properties are very different. The temperature dependence of the resistivity is suggestive of a degenerate semiconductor with a 290-K resistivity of ~40 Ω cm, and a maximum –MR of 2% is reported in a 9-T field. A variable temperature synchrotron diffraction study was also performed on beamline ID31 at the ESRF, and there is no evidence of anomalies in the cell parameters or bond lengths between 4 and 250 K.[37] This is in contrast to the results described here, where NdMnAsO is a disordered semiconductor (290-K resistivity = 1268 Ω cm) with a sizable –MR over a wide temperature range[25] and exhibits an electronic transition at 150 K, which appears to be coupled to the crystal lattice (Figs. 4–6). Both samples are of similar quality, and the only difference appears to be the nonstoichiometry of the L site in GMR LMnAsO samples (L = Nd and La; Tables SIII and IV). To investigate this further we have synthesized three Nd_xMnAsO samples with different x and recorded the temperature variation of the 5-T MR (Fig. 7). It is clear that the MR properties of Nd_xMnAsO are strongly stoichiometry dependent, so that the magnitude of –MR decreases with increasing x. Upon increasing x from 0.970 to 0.988 in Nd_xMnAsO, the electronic properties change from a disordered semiconductor to a degenerate semiconductor with 290-K resistivity equal to 105 and 41 Ω cm for $x = 0.988$ and 1.00, respectively. The large increase in resistivity upon decreasing x may then be explained by trapping of the carriers by the cation disorder (Anderson localization). Negative MR arising from a reduction in QDI with field is only observed in highly disordered semiconductors, and it appears that the Nd nonstoichiometry in the materials reported here establishes this disorder. Another implication of these findings is that it may be possible to tune the –MR by further reduction in x, and further research is warranted.

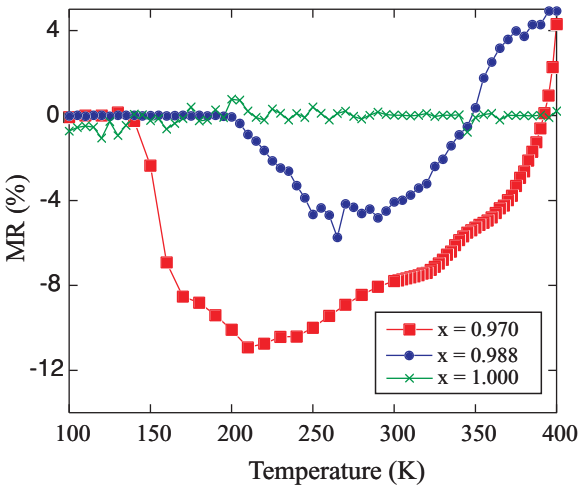

FIG. 7. (Color online) Variation of 5-T MR with temperature for three different Nd_xMnAsO samples.

In summary, we report that NdMnAsO exhibits a spin reorientation from alignment parallel to c above T_N (Nd) to alignment along the basal plane below T_N (Nd). This further illustrates the strong interplay between the lanthanide and transition-metal magnetism in LMAsO oxypnictides. A structural response is evident at T_e, where clear discontinuities in L-O and Mn-As bond lengths are observed. It is surprising that the electronic transition is manifest in both the L-O and Mn-As bond lengths and suggests that there may be electronic as well as magnetic coupling between the two layers. The results show that the electronic properties of LMnAsO are strongly dependent on the nonstoichiometry of the L site, whereas the magnetic properties are relatively unaffected.

ACKNOWLEDGEMENT

We acknowledge the UK EPSRC for financial support and STFC-GB for provision of beamtime at ISIS and ESRF.

*a.c.mclaughlin@abdn.ac.uk

[1] J. G. Bednorz and K. A. Muller, Z. Phys. B **64**, 189 (1986).

[2] Y. Kamihara, T. Watanabe, M. Hirano, and H. Hosono, J. Am. Chem. Soc. **130**, 3296 (2008).

[3] G. F. Chen, Z. Li, D. Wu, J. Dong, G. Li, W. Z. Hu, P. Zheng, J. L. Luo, and N. L. Wang, Chin. Phys. Lett. **25**, 2235 (2008).

[4] Z. A. Ren, J. Yang, J. W. Lu, W. Yi, G. C. Che, X. L. Dong, L. L. Sun, and Z. X. Zhao, Mater. Res. Innov. **12**, 105 (2008).

[5] R. Pottgen and D. Johrendt, Z. Naturforsch. **63b**, 1135 (2008).

[6] Z.-A. Ren, G.-Can. Che, X.-L. Dong, J. Yang, W. Lu, W. Yi, X.-L. Shen, Z.-C. Li, L.-L. Sun, F. Zhou, and Z.-X. Zhao, Europhys. Lett. **83** 17002 (2008).

[7] C. de la Cruz, Q. Huang, J. W. Lynn, J. Li, W. Ratcliff, J. L. Zarestky, H. A. Mook, G. F. Chen, J. L. Luo, N. L. Wang, and P. Dai, Nature (London) **453**, 899 (2008).

[8] H.-H. Wen, G. Mu, L. Fang, H. Yang, and X. Zhu, Europhys. Lett. **82**, 17009 (2008).

[9] K. Kasperkiewicz, J.-W. G. Bos, A. N. Fitch, K. Prassides, and S. Margadonna, Chem. Commun. **6**, 707 (2009).

[10] G. Cao, S. Jiang, X. Lin, C. Wang, Y. Li, Z. Ren, Q. Tao, C. Feng, J. Dai, Z. Xu, and F. C. Zhang, Phys. Rev. B **79**, 174505 (2009).

[11] A. S. Sefat, A. Huq, M. A. McGuire, R. Jin, B. C. Sales, D. Mandrus, L. M. D. Cranswick, P. W. Stephens, and K. H. Stone, Phys. Rev. B **78**, 104505 (2008).

[12] Z. Li, G. Chen, J. Dong, G. Li, W. Hu, D. Wu, S. Su, P. Zheng, T. Xiang, N. Wang, and J. Luo, Phys. Rev. B **78**, 060504 (2008).

[13] H. Yanagi, R. Kawamura, T. Kamiya, Y. Kamihara, M. Hirano, T. Nakamura, H. Osawa, and H. Hosono, Phys. Rev. B **77**, 224431 (2008).

[14] A. Marcinkova, D. A. M. Grist, I. Margiolaki, T. C. Hansen, S. Margadonna, and J.-W. G. Bos, Phys. Rev. B **81**, 064511 (2010).

[15] M. A. McGuire, D. J. Gout, V. O. Garlea, A. S. Sefat, B. C. Sales, and D. Mandrus, Phys. Rev. B **81**, 104405 (2010).

[16] A. Leithe-Jasper, W. Schnelle, C. Geibel, and H. Rosner, Phys. Rev. Lett. **101**, 207004 (2008).

[17] K. Sasmal, B. Lv, B. Lorenz, A. M. Guloy, F. Chen, Y. Y. Xue, and C.-W. Chu, Phys. Rev. Lett. **101**, 107007 (2008).

[18] G. F. Chen, Z. Li, G. Li,W. Z. Hu, J. Dong, X. D. Zhang, P. Zheng, N. L. Wang, and J. L. Luo, Chin. Phys. Lett. **25**, 3403 (2008).

[19] A. S. Sefat, D. J. Singh, R. Jin, M. A. McGuire, B. C. Sales, and F. Roning, Physica C **469**, 350 (2009).

[20] N. Kurita, F. Ronning, Y. Tokiwa, E. D. Bauer, A. Subedi, D. J. Singh, J. D. Thompson, and R. Movshovich, Phys. Rev. Lett. **102**, 147004 (2009).

[21] A. S. Sefat, D. J. Singh, R. Jin, M. A. McGuire, B. C. Sales, and D. Mandrus, Phys. Rev. B **79**, 024512 (2009).

[22] M. Rotter, M. Tegel, and D. Johrendt, Phys. Rev. Lett. **101**, 107006 (2008).

[23] Y. Singh, M. A. Green, Q. Huang, A. Kreyssig, R. J. McQueeney, D. C. Johnston, and A. I. Goldman, Phys. Rev. B **80**, 100403 (2009).

[24] Y. Singh, A. Ellern, and D. C. Johnston, Phys. Rev. B **79**, 094519 (2009).

[25] N. Emery, E. J. Wildman, J. M. S. Skakle, G. Giriat, R. I. Smith, and A. C. Mclaughlin, Chem. Commun. **46**, 6777 (2010).

[26] H. M. Rietveld, Acta Crystallogr. **22**, 151 (1967).

[27] A. C. Larson and R. B. Von Dreele, General Structure Analysis System (GSAS), Los Alamos National Laboratory, Technical Report No. LAUR86-748, 2004 (unpublished).

[28] See supplemental material at [http://link.aps.org/supplemental/10.1103/PhysRevB.83.144429] for Rietveld refinement figures and tables of crystallographic data.

[29] A. S. Wills, Physica B 276, **680** (2000), program available from [www.ccp14.ac.uk].

[30] R. Sachidanandam, T. Yildirim, A. B. Harris, A. Aharony, and O. Entin-Wohlman, Phys. Rev. B **56**, 260 (1997).

[31] N. Manyala, Y. Sidis, J. D. Ditusa, G. Aeppli, D. P. Young, and Z. Fisk, Nature (London) **404**, 581 (2000).

[32] *Colossal Magnetoresistance, Charge Ordering and Related Properties of Manganese Oxides*, edited by C. N. R. Rao and B. Raveau (World Scientific, Singapore, 1998).

[33] A. T. Nientiedt, W. Jeitschko, P. G. Pollmeier, and M. Brylak, Z. Naturforsch. **52b**, 560 (1997).

[34] S. Srinath, M. M. Kumar, M. L. Post, and H. Srikanth, Phys. Rev. B **72**, 054425 (2005).

[35] P. S. Prabhu, M. S. Ramachandra Rao, U. V. Varadaraju, and G. V. Subba Rao, Phys. Rev. B **50**, 6929 (1994).

[36] V. Vildosola, L. Pourovskii, R. Arita, S. Biermann, and A. Georges, Phys. Rev. B **78**, 064518 (2008).

[37] A. Marcinkova, T. C. Hansen, C. Curfs, S. Margadonna, and J.-W. G. Bos, Phys. Rev. B **82**, 174438 (2010).